
PAI-GCN: Permutable Anisotropic Graph Convolutional Networks for 3D Shape Representation Learning

Zhongpai Gao¹ Guangtao Zhai¹ Juyong Zhang² Yiyang Yang¹ Xiaokang Yang¹

Abstract

Demand for efficient 3D shape representation learning is increasing in many 3D computer vision applications. The recent success of convolutional neural networks (CNNs) for image analysis suggests the value of adapting insight from CNN to 3D shapes. However, unlike images that are Euclidean structured, 3D shape data are irregular since each node’s neighbors are inconsistent. Various convolutional graph neural networks for 3D shapes have been developed using isotropic filters or using anisotropic filters with predefined local coordinate systems to overcome the node inconsistency on graphs. However, isotropic filters or predefined local coordinate systems limit the representation power. In this paper, we propose a permutable anisotropic convolutional operation (PAI-Conv) that learns adaptive soft-permutation matrices for each node according to the geometric shape of its neighbors and performs shared anisotropic filters as CNN does. Comprehensive experiments demonstrate that our model produces significant improvement in 3D shape reconstruction compared to state-of-the-art methods.

1. Introduction

3D shape representation learning is crucial for many 3D computer vision tasks, such as 3D reconstruction (Genova et al., 2018; Tran & Liu, 2018), shape synthesis and modeling (Cao et al., 2014b; Xie et al., 2018), 3D object classification and segmentation (Kalogerakis et al., 2010; Qi et al., 2017), as well as graphics applications such as virtual avatar (Cao et al., 2014a). Inspired by the great success of convolutional neural networks (CNN) in the fields of natural language processing, object detection and tracking, and medical image analysis where underlying data are Euclidean structured, deep neural networks on 3D geometric data (e.g.,

mesh and point cloud) have recently driven significant interests. Directly applying CNN on 3D geometric data is a challenge since they are non-Euclidean structured and are usually represented as graphs in which the number and orientation of each node’s neighbors vary from one to another (node inconsistency). An effective definition of convolutional operation analogous to that on Euclidean structured data is important for 3D shape representation learning.

Recently, many graph convolutional networks have been developed to handle irregular graph data and achieved promising results. Michaël Defferrard et al., (2016) designed fast localized convolutional filters on graphs using Chebyshev expansion based on spectral graph theory, called *ChebNet*. The spectral filters are isotropic and permutation invariant to overcome the irregularity of graph data. ChebNet is an efficient generalization of CNNs to graphs. Anurag Ranjan et al., (2018) built convolutional mesh autoencoder (COMA) upon ChebNet and introduced mesh sampling operations that enable a hierarchical mesh representation to capture non-linear variations of human faces. However, different from CNNs that use anisotropic filters to extract local features, isotropic filters of spectral convolutions limit the representation power.

In order to introduce anisotropic filters on graph convolutions, Giorgos Bouritsas et al., (2019) formulated a spiral convolution operator (Spiral-Conv) that defines a local neighborhood around each vertex on the mesh, by enforcing an explicit ordering of the neighbors via a spiral scan. However, this method requires manually assigning a starting point to fix the orientation and ordering of neighbors. The selection of the starting point may affect the performance of the spiral convolution operator. Moreover, explicitly defining the ordering of neighbors cannot efficiently exploit the irregular structure of graphs.

In this paper, we propose a permutable anisotropic convolutional operator (*PAI-Conv*) for 3D meshes. For each vertex, instead of processing convolution directly on the vertex neighbors, the convolutional neighbors are obtained by resampling the vertex’s neighbors with a soft permutation matrix that is trained along with the networks. Then similar to CNNs, we apply shared anisotropic filters on the convolutional neighbors to extract local features on meshes.

¹Artificial Intelligence Institute, Shanghai Jiao Tong University, Shanghai, China ²University of Science and Technology of China, Anhui, China. Correspondence to: Zhongpai Gao <gaozhongpai@sjtu.edu.cn>.

PAI-Conv is designed to learn adaptive soft permutation matrices without explicitly defining the ordering of neighbors and can be applied to arbitrary mesh topologies and point clouds for 3D shape representation learning.

PAI-Conv is easy to implement and integrate into existing deep learning models to improve their performance. We use PAI-Conv to build convolutional mesh autoencoder and achieve state-of-the-art performance on two 3D shape datasets: human faces (COMA (Ranjan et al., 2018)) and human bodies (DFAUST (Bogo et al., 2017)). Comprehensive evaluation experiments show that the proposed method significantly outperforms existing models. The main contributions of this paper are summarized below:

- We propose a novel convolution operation for representation learning from 3D shapes, **permutable anisotropic convolution (PAI-Conv)**, to better capture local geometric features of 3D shapes.
- We show that PAI-Conv can be implemented and integrated into existing pipelines for 3D shape processing.
- Extensive experiments show that our model achieves state-of-the-art performance for 3D shape generations.

2. Related work

Linear 3D morphable models 3D morphable models (3DMM) are statistical models of 3D shapes, such as human faces, bodies, hands, etc., and are constructed by performing some form of dimensionality reduction on a training set that each mesh is in dense correspondence with each other (i.e., fixed topology). 3DMMs are powerful priors on 3D shape reconstruction or generation. Blanz & Vetter (Blanz & Vetter, 1999b) proposed the first linear parametric 3DMM using principal component analysis (PCA) to model the shape and texture of 3D faces. The widely used 3DMM for faces (Zhu et al., 2015) was built by merging Basel Face Model (BFM) (Paysan et al., 2009) with 200 subjects in neutral expressions and FaceWarehouse (Cao et al., 2014b) with 150 subjects in 20 different expressions. Skinned multi-person linear model (SMPL) (Loper et al., 2015) is the most well known body model that was learned through PCA and represents a wide variety of body shapes in natural human poses. MANO (Romero et al., 2017) is a hand model that learned from around 1000 high-resolution 3D scans of human hands in a wide variety of hand poses. Those PCA-based models are commonly used for 3D faces, bodies, and hands reconstruction. In this paper, we introduce a non-linear 3DMM for 3D shapes with better representation power.

Geometric deep learning The popularity of extending deep learning approaches for graph data has been rapidly growing in recent years. Convolutional graph neural networks fall into two categories: spectral-based and spatial-based.

Spectral-based approaches define convolution operation based on graph signal processing. For example, spectral CNN (Bruna et al., 2014) generalize convolution to graphs via Laplacian eigenvectors. ChebNet (Defferrard et al., 2016) and GCN (Kipf & Welling, 2017) reduce the computation complexity of eigen-decomposition by using fast localized convolutional filters. AGCN (Li et al., 2018) learns hidden structural relations unspecified by the graph adjacency matrix. DualGCN (Zhuang & Ma, 2018) introduces a dual graph convolutional architecture with two graph convolutional layers in parallel. Spatial-based approaches define graph convolutions based on a node’s spatial relations. For example, DCNN (Atwood & Towsley, 2016) assumes information is transferred from one node to its neighbors with a certain transition probability and regards graph convolutions as a diffusion process. GraphSage (Hamilton et al., 2017) adopts sampling to obtain a fixed number of neighbors for each node. GAT (Veličković et al., 2018) adopts attention mechanisms to learn the relative weights between two connected nodes. MoNet (Monti et al., 2017) introduces node pseudo-coordinates to determine the relative position between a node and its neighbors and assigns different weights to the node’s neighbors. In this paper, we propose a novel spatial-based approach for deep learning on 3D shape data.

3. Our approach

Inspired by the conventional convolution on Euclidean structured data, we propose a permutable anisotropic convolutional operation (PAI-Conv) on graphs. Instead of directly applying anisotropic filters on each node’s neighbors, we resample each node’s neighbors using a soft permutation matrix that is trained along with the deep neural networks.

3.1. Permutable anisotropic convolution

Consider a 3D shape that is described as a mesh $M = (\mathcal{V}, \mathcal{E})$, where $\mathcal{V} = \{1, \dots, N\}$ is a set of vertices and $\mathcal{E} \subseteq \mathcal{V} \times \mathcal{V}$ is a set of edges. A graph may have node attributes $\mathbf{X} \in \mathbb{R}^{D \times N}$, where D and N represents the feature dimension and number of nodes, respectively. In the simplest setting of $D = 3$, each node contains 3D coordinates $\mathbf{x}_i = [x_i, y_i, z_i]^T$ in the Euclidean space. The node attributes can also include additional coordinates such as color and vertex normal. In a deep neural network, the output of each layer is as the input for the subsequent layer. Thus, generally, D represents the feature dimension of a given layer in the deep neural network.

We define PAI-Conv as follows. For each node, \mathcal{N}_i is a set of the one-ring neighborhood of \mathbf{x}_i (including itself), where $\mathbf{x}_j \in \mathcal{N}_i$ and $(\mathbf{x}_i, \mathbf{x}_j) \in \mathcal{E}$. We denote $\mathcal{N}_i = \{\mathbf{x}_i, \mathbf{x}_{i,1}, \dots, \mathbf{x}_{i,|\mathcal{N}_i|-1}\}$, where $|\mathcal{N}_i|$ is the number of node’s neighbors and it varies from one node to

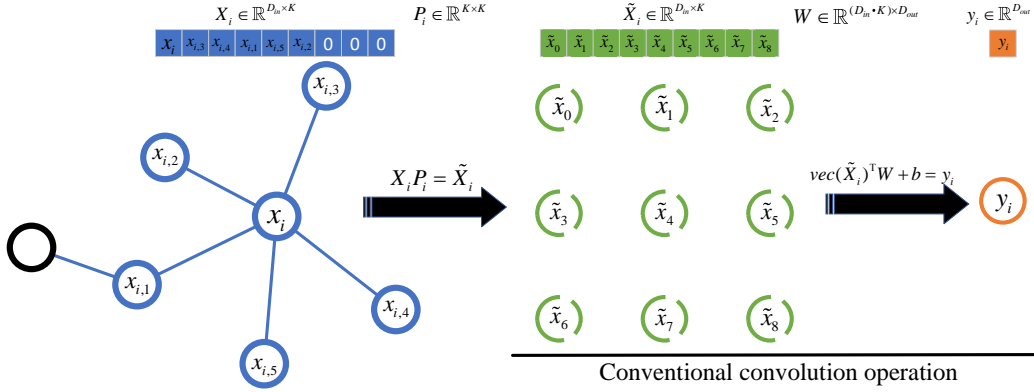


Figure 1. Permutable anisotropic convolutional operation (PAI-Conv). $\{x_i, x_{i,1}, \dots, x_{i,5}\} \subseteq \mathcal{N}_i$ are the one-ring neighborhood of x_i (including itself). We construct $X_i = \{x_i, x_{i,1}, \dots, x_{i,K-1}\} \in \mathbb{R}^{D_{in} \times K}$ where K is a predefined neighbor size, e.g., $K = 9$. PAI-Conv has two steps. First, a learnable soft-permutation matrix, $P_i \in \mathbb{R}^{K \times K}$ is used to resample the node’s neighbors. Second, a conventional convolution operation with anisotropic filters, $W \in \mathbb{R}^{(D_{in} \cdot K) \times D_{out}}$, is performed. $b \in \mathbb{R}^{D_{out}}$ is the bias.

another in a graph. In order to apply a shared anisotropic filter on each node, we define a constant neighbor size K , which is analogue to the kernel size in conventional convolution operation. For each node, we construct $X_i = \{x_i, x_{i,1}, \dots, x_{i,K-1}\} \in \mathbb{R}^{D_{in} \times K}$, where the first K neighbors are selected if K is smaller than or equal to $|\mathcal{N}_i|$; otherwise zero-padding is applied, as shown in Figure 1. Note that, we put the node itself, x_i , in the first place and the ordering of other neighbors $\{x_{i,1}, \dots, x_{i,K-1}\}$ in X_i is random and without specified.

Since the order and orientation of neighbors for each node vary from one to another, directly applying an anisotropic filter on unordered neighbors diminishes the representation power. While training, the anisotropic filter might struggle to adapt to the large variability of the unordered coordinate systems and the possibility of learning rotation invariant filter increases. In this paper, we introduce an adaptive soft-permutation matrix to resample the neighbors of each node, denoted as $P_i \in \mathbb{R}^{K \times K}$. The resampled convolutional neighbors of each node can be obtained by

$$\tilde{X}_i = X_i P_i, \quad (1)$$

where $\tilde{X}_i \in \mathbb{R}^{D_{in} \times K}$ and P_i is a trainable parameter to be adaptive according to the geometric structure of the node’s neighbors.

We assume that the learned soft-permutation matrix for each node is able to resample the node’s neighbors with weights so that we can apply a shared anisotropic filter on each node of a graph. This operation is the same as the conventional convolution and can be expressed as

$$y_i = \text{vec}(\tilde{X}_i)^\top W + b, \quad (2)$$

where $W \in \mathbb{R}^{(D_{in} \cdot K) \times D_{out}}$ includes D_{out} anisotropic filters, $b \in \mathbb{R}^{D_{out}}$ is the bias, $y_i \in \mathbb{R}^{D_{out}}$ is the output feature

node corresponding to the input node $x_i \in \mathbb{R}^{D_{in}}$, and $\text{vec}(\cdot)$ is a vectorization function which converts a matrix into a column vector. In order to introduce non-linearity, an activation function $f(\cdot)$ such as ELU (Clevert et al., 2015) is introduced on Eq (1) and (2). Thus, PAI-Conv is defined as

$$y_i = f(\text{vec}(f(X_i P_i))^\top W + b). \quad (3)$$

Note that, a graph’s each node has a corresponding soft-permutation matrix and all nodes share the same anisotropic filter for each output channel.

3.2. Properties

Intuitively, **anisotropic filter** and **permutation invariance** are two mutually exclusive properties. Using anisotropic filter requires each node’s neighbors are sorted in a certain way while permutation invariance means we can randomly change the order of each node’s neighbors. However, PAI-Conv resolves these two incompatible properties by introducing learnable soft-permutation matrices so that the initial order of each node’s neighbors is not important.

3.3. Comparison to existing methods

Isaak Lim et al. (2018) and Giorgos Bouritsas et al., (2019) construct intrinsic operators that define a local neighborhood around each vertex on the mesh by enforcing an explicit ordering of the neighbors via a spiral scan. In Giorgos Bouritsas et al., (2019), each node’s neighbors are constructed as $X_i = \{x_i, x_{i,1}, \dots, x_{i,K-1}\} \in \mathbb{R}^{D_{in} \times K}$, where $(x_i, x_{i,1}, \dots, x_{i,K-1})$ are sorted in a predefined spiral order. The spiral convolution is defined as

$$y_i = f(\text{vec}(X_i)^\top W + b). \quad (4)$$

However, the number of each node’s neighbors varies from one to another. The orientations and distances of each node’s

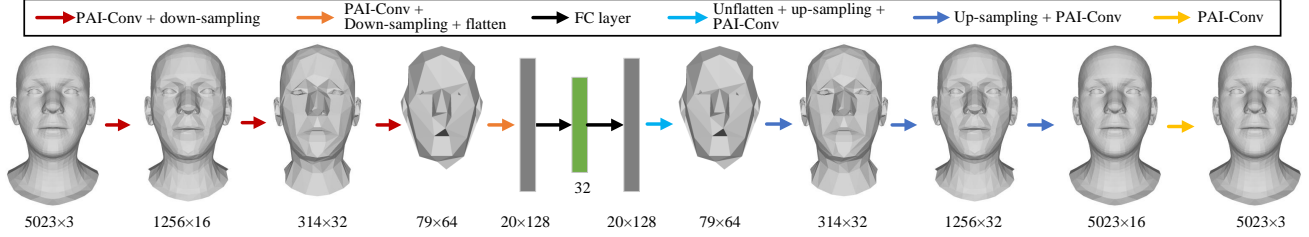


Figure 2. Architecture of our PAI-Conv based 3D morphable models (PAI-3DMM).

neighbors to the node also change from one to another. Serializing the local neighborhood of vertices by following a spiral cannot resolve the inconsistency between different nodes. Moreover, it is difficult to choose a starting point for each spiral in order to make the local coordinate system consistent across meshes.

ChebNet (Defferrard et al., 2016) and GCN (Kipf & Welling, 2017) developed spectral convolutional operators for graphs. For GCN, the spectral composition is defined as

$$\mathbf{Y} = f(\hat{\mathbf{A}}\mathbf{X}\Theta), \quad (5)$$

where $\hat{\mathbf{A}} = \tilde{\mathbf{D}}^{-\frac{1}{2}}\tilde{\mathbf{A}}\tilde{\mathbf{D}}^{-\frac{1}{2}}$ with $\tilde{\mathbf{A}} = \mathbf{A} + \mathbf{I}_N$ and $\tilde{\mathbf{D}}_{i,i} = \sum_j \tilde{\mathbf{A}}_{i,j}$ and $\mathbf{A} \in \mathbb{R}^{N \times N}$ is the sparse adjacency matrix representing the edge connections, $\Theta \in \mathbb{R}^{D_{in} \times D_{out}}$ is a learnable isotropic filter parameter, $\mathbf{X} \in \mathbb{R}^{N \times D_{in}}$ is the input feature nodes, and $\mathbf{Y} \in \mathbb{R}^{N \times D_{out}}$ is the output graph nodes. The spectral convolutional operators use isotropic filters to overcome the non-canonical ordering of the neighbor vertices, which largely diminishes the representation power compared to the conventional convolution operator on Euclidean data.

MoNet (Monti et al., 2017) introduce a local “pseudo-coordinate system” \mathbf{u} in which the neighborhood vertices are represented and a weight function (kernel) is defined. Under MoNet framework, several existing approaches for 3D shapes such as Geodesic CNN (Masci et al., 2015), Anisotropic CNN (Boscaini et al., 2016), and even GCN (Kipf & Welling, 2017) can be generalized as special instances of MoNet by constructing nonparametric weight function. MoNet convolution is defined as an M-component Gaussian mixture

$$\mathbf{y}_{im} = \sum_{j:(i,j) \in \mathcal{E}} \theta_m \cdot (\mathbf{x}_j \odot g_{w_n}(\mathbf{u}(\mathbf{x}_i, \mathbf{x}_j))), \quad (6)$$

where g_{w_n} is a Gaussian kernel with learnable parameters of Gaussian’s mean and covariance, $\theta = \{\theta_1, \dots, \theta_{D_{out}}\}$ are the learnable filters, and \odot is Hadamard product. Different from MoNet, PAI-Conv does not need to construct a local “pseudo-coordinate system” manually, but directly learns a soft-permutation matrix for each node according to the geometric shape around the node. With the resampled convolutional neighbors, anisotropic filters are able to take

effect on improving the representation power compared to isotropic filters.

3.4. PAI-Conv based 3D morphable models

In this paper, we propose a nonlinear 3D morphable model using our PAI-Conv as building blocks, called *PAI-3DMM*. The basic architecture of PAI-3DMM is the same as COMA (Ranjan et al., 2018) and Spiral (Bouritsas et al., 2019), as shown in Figure 2. We simply replace the convolutional operations (i.e., ChebNet or Spiral-Conv) with PAI-Conv. PAI-3DMM is a deep convolutional mesh autoencoder with hierarchical mesh representations and is able to capture nonlinear variations in 3D shapes at multiple scales within the model.

We denote as $FC(\cdot)$ a fully connected layer, d the dimension of latent vector, l the number of vertices after the last down-sampling layer, $PC(k, c)$ a PAI-Conv layer with neighbor size k and number of filters c , $DS(p)$ a down-sampling layer by a factor of p , and $US(p)$ a up-sampling layer by a factor of p , respectively. PAI-3DMM is listed as follows:

$$\begin{aligned} enc : & PC(9, 16) \rightarrow DS(4) \rightarrow PC(9, 32) \rightarrow DS(4) \rightarrow \\ & PC(9, 64) \rightarrow DS(4) \rightarrow PC(9, 128) \rightarrow DS(4) \rightarrow FC(d), \\ dec : & FC(l * 128) \rightarrow US(4) \rightarrow PC(9, 64) \rightarrow US(4) \rightarrow \\ & PC(9, 32) \rightarrow US(4) \rightarrow PC(9, 32) \rightarrow US(4) \rightarrow \\ & PC(9, 16) \rightarrow PC(9, 3). \end{aligned}$$

The model’s encoder effectively compresses a 3D shape into a low dimensional latent vector (e.g., $d = 32$ in Figure 2) and the decoder reconstructs the 3D shape from the latent vector. PAI-3DMM can be used in 3D shape recognition, reconstruction, and many other applications.

4. Evaluation

In this section, we first evaluate the proposed model on two different 3D shape datasets by comparing to state-of-the-art approaches. Then, a parameter reduction method is proposed for PAI-Conv. At last, ablation tests are conducted to demonstrate the effectiveness of PAI-Conv.

Datasets We evaluate our model on two datasets: COMA (Ranjan et al., 2018) and DFAUST (Bogo et al., 2017).

COMA is a human facial dataset that consists of 12 classes of extreme expressions from 12 different subjects. The dataset contains 20,466 3D meshes that were registered to a common reference template with 5023 vertices. DFAUST is a human body dataset that collects over 40,000 real meshes, capturing 129 dynamic performances from 10 subjects. A mesh registration method that uses both 3D geometry and texture information to register all scans in a sequence to a common reference topology with 6890 vertices. The same as in (Ranjan et al., 2018), we split both two datasets into training and test set with a ratio of 9:1 and randomly select 100 samples from the training set for validation. We perform standardization on all the 3D shape meshes by subtracting the mean shape and dividing with each vertex’s standard deviation to improve the convergence speed of training.

Training We use Adam (Kingma & Ba, 2014) optimizer with learning rate 0.001 and reduce the learning rate with decay rate 0.99 in every epoch. The batch size is 32 and total epoch number is 300. We initialize the soft-permutation matrices with identity matrix, $I \in \mathbb{R}^{K \times K}$, i.e., the network starts without resampling the node’s neighbors. Weight decay regularization is used for the network parameters except for the soft-permutation matrices.

4.1. Comparison to existing methods

We compare three existing methods: PCA (Blanz & Vetter, 1999a), COMA (Ranjan et al., 2018), and Spiral (Bouritsas et al., 2019) on different dimensionalities of the latent space: 8, 16, 32, 64, and 128. The same architecture in Figure 2 is used in the methods of COMA, Spiral, and our PAI-3DMM for consistency and fair comparison. As shown in Figure 3, the proposed PAI-3DMM achieves the smallest reconstruction errors compared to COMA and Spiral on both COMA and DFAUST datasets by a large margin. PAI-3DMM consistently cuts the errors by around half for all the dimensionalities of latent space on both two datasets thanks to the proposed PAI-Conv operation. PAI-Conv significantly improves the expressive power on 3D shape representation learning compared to ChebNet and Spiral-Conv.

Compared to PCA, all the methods based on deep neural networks (DNN) have smaller reconstruction errors for a small latent size ($d < 32$). This is because PCA-based linear 3DMMs can only capture global features and DNN-based nonlinear 3DMMs are able to capture local features using convolutional operations. The reconstruction accuracy of PAI-3DMM is comparable to PCA even when the latent size is 128. Note that, the latent size in 3DMMs should be small for the purpose of dimension reduction for some downstream applications. Moreover, large latent sizes in 3DMMs may lead to less semantically meaningful representations of 3D shapes.

Figure 4 shows the training and validation reconstruction er-

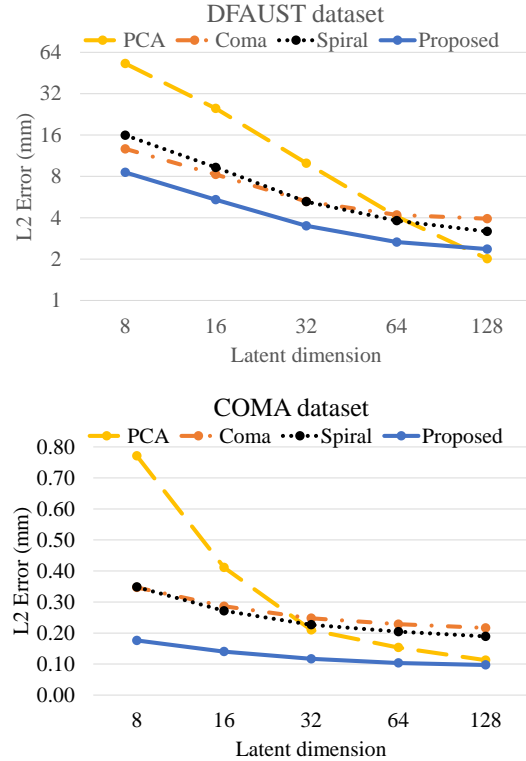


Figure 3. Quantitative evaluation of our PAI-3DMM against the existing methods: PCA, COMA, and Spiral from the test sets.

rors for the methods of COMA, Spiral, and our PAI-3DMM with the latent size of 32. The results of COMA and Spiral are rather close to each other: COMA performs slightly better on DFAUST dataset and Spiral performs slightly better on COMA dataset. Our PAI-3DMM converges much faster than COMA and Spiral. As shown in Figure 4d, after training for only 5 iterations, PAI-3DMM achieves smaller reconstruction error than COMA and Spiral training for 300 iterations.

In Figure 5, we qualitatively compare the reconstruction errors of some examples from the test sets of DFAUST and COMA datasets with the latent size $d = 32$. Our PAI-3DMM achieves smaller reconstruction errors for each case from the test sets. It is clearly visible that PCA has the largest reconstruction errors on DFAUST dataset (Figure 5a) and Spiral has the largest reconstruction errors on COMA dataset (Figure 5b), which is consistent with the data shown in Figure 3. For Spiral, even though anisotropic filters are used compared to COMA that uses isotropic filters, the improvement is very limited since the manually designed neighbor ordering cannot define the local coordinates very well. In contrast, our learnable soft-permutation matrices can resample each node’s neighbors that cooperate well with the shared anisotropic filters to extract local features of 3D shapes. As a result, PAI-3DMM performs better for 3D

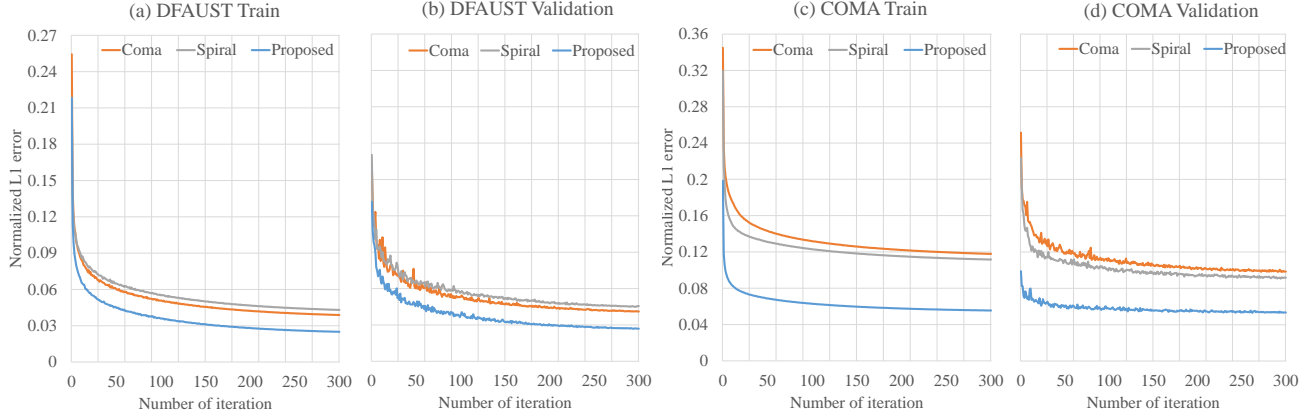


Figure 4. Training and validation reconstruction errors on COMA and DFAUST datasets when the latent size $d = 32$.

shape representation learning.

4.2. Parameter reduction for PAI-3DMM

Note that, in order to learn the soft-permeation matrix for each node, the number of parameters of our model is relatively large. For example, when the neighbor size is $K = 9$, the number of parameters of those soft-permeation matrices for COMA dataset is $(5023 \times 3 + 1256 \times 2 + 314 \times 2 + 79 \times 2 + 20 \times 2) \times 9 \times 9 = 1,490,967$ (Figure 2). When the latent size is $d = 32$, the parameter numbers of our model and PCA model are 1,867K and 482K, respectively. However, our model achieves much better reconstruction accuracy compared to PCA: $0.117mm$ vs. $0.21mm$. The proposed model is the choice for situations that require low reconstruction errors and do not strictly limit the model size. Usually, increasing the model size by around 1M is not an issue while improving reconstruction accuracy is crucial for many applications.

We also provide a method to reduce the number of our model’s parameters for situations where the model size should be limited. When the number of nodes is large, it is not necessary to learn the soft-permutation matrix for each node since the geometric shapes of many nodes are similar to each other. We assume that the soft-permutation matrices for all the nodes fall into a smaller subspace. We apply a matrix factorization technique in PAI-Conv. For a mesh with N nodes, we denote $\mathbf{P} \in \mathbb{R}^{N \times K \times K}$ for all the soft-permutation matrices that can be factorized as follows,

$$\mathbf{P} = \mathbf{V}\mathbf{P}_b, \quad (7)$$

where $\mathbf{P}_b \in \mathbb{R}^{B \times K \times K}$ is the B -dimensional subspace’s bases of soft-permutation matrices, $\mathbf{V} \in \mathbb{R}^{N \times B}$ is the corresponding weights for the N nodes, and $B \ll N$ (e.g., $N = 5023, B = 8$). Instead of learning N soft-permutation matrices directly, we learn a small number of soft-permutation matrix bases and each node’s corre-

Table 1. Comparison of reconstruction errors for the models of PCA, COMA, Spiral, and our PAI-3DMM with latent size $d = 32$. *PAI (small)* is the model of PAI-3DMM with parameter reduction, where the dimension of soft-permutation matrix subspace $B = 8$. COMA (v2) and Spiral (v2) are the models with increasing feature size to have around the same parameter number with *PAI (small)*.

DATASET	METHOD	L2 ERROR (MM)	# OF PARM
DFAUST	SAME ARCHITECTURE		
	PCA	9.977	661K
	COMA	5.238	361K
	SPIRAL	5.258	446K
	PAI-3DMM	3.492	2,478K
	SAME # OF PARM		
	COMA (v2)	5.110	658K
SPIRAL (v2)	4.667	647K	
PAI (small)	4.544	644K	
COMA	SAME ARCHITECTURE		
	PCA	0.210	482K
	COMA	0.248	303K
	SPIRAL	0.227	414K
	PAI-3DMM	0.117	1,867K
	SAME # OF PARM		
	COMA (v2)	0.198	532K
SPIRAL (v2)	0.193	533K	
PAI (small)	0.179	532K	

sponding weight, which can largely reduce the number of parameters depending on the choice of B .

Table 1 shows the comparison of reconstruction errors for models with different parameter numbers on DFAUST and COMA datasets. When using the same architecture (Figure 2), PAI-3DMM has the smallest reconstruction errors. We use the technique of matrix factorization for the soft-permutation matrices to reduce the parameter number of our PAI-3DMM, denoted as *PAI (small)*. When the subspace dimension $B = 8$, the model’s parameter numbers on DFAUST and COMA datasets reduce from 2,478K to 644K

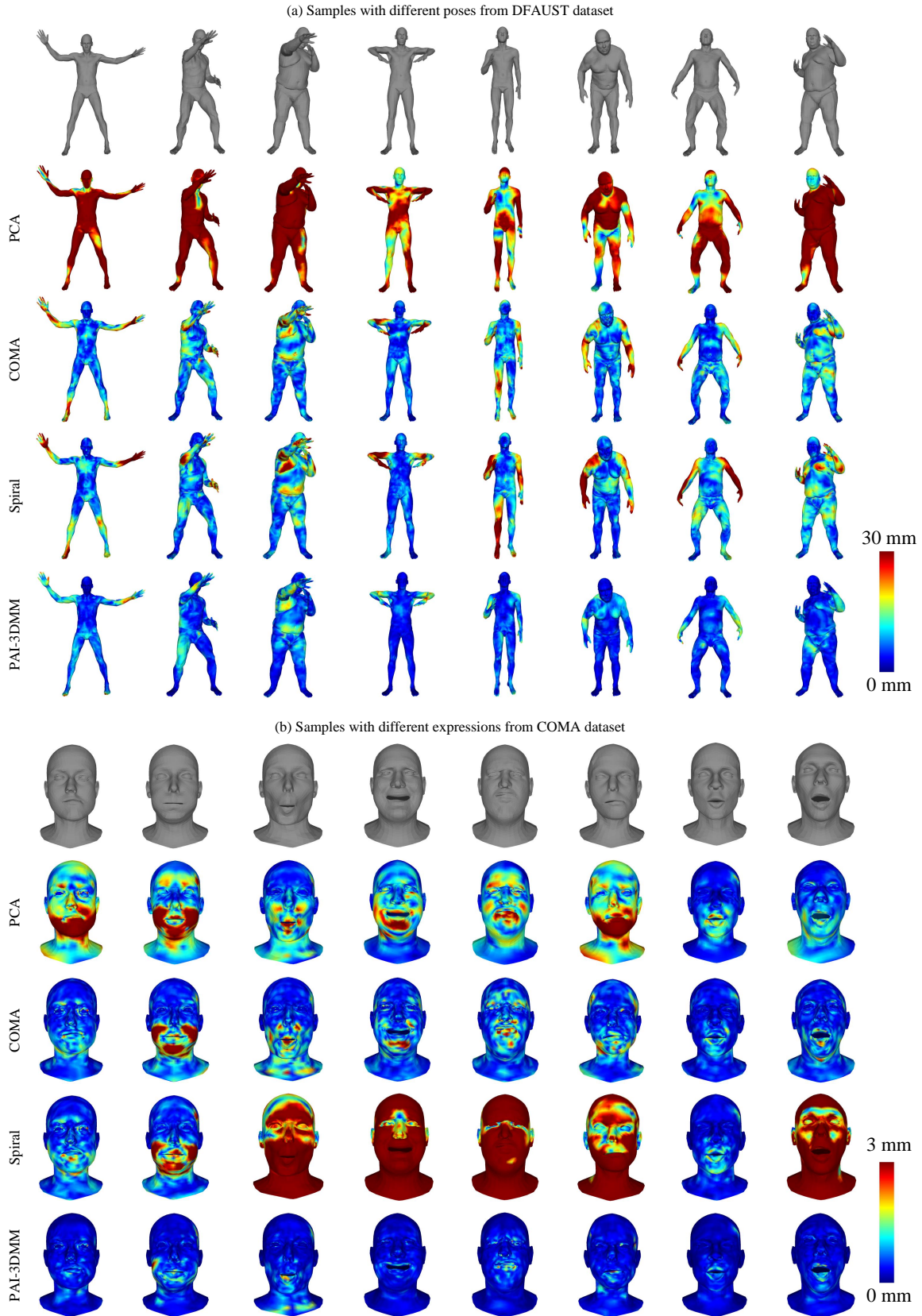


Figure 5. Colormaps of per vertex Euclidean error of the reconstructions produced by PCA (2nd), COMA (3rd), Spiral (4th), and our PAI-3DMM (bottom). Top row is the ground truth meshes from test sets. The latent size of the models is 32.

and from 1,867K to 532K, respectively. In order to have a fair comparison, we increase the feature sizes of COMA and Spiral so that the models have around the same number of parameters, denoted as *COMA* ($v2$) and *Spiral* ($v2$). The feature sizes in *COMA* ($v2$) are [64, 96, 112, 128] and [128, 112, 96, 96, 64]; The feature sizes in *Spiral* ($v2$) are [32, 64, 64, 128] and [128, 110, 64, 64, 32]; while the feature sizes in *PAI* (*small*) are [16, 32, 64, 128] and [128, 64, 32, 32, 16]. As shown in Table 1, under the same parameter size, *PAI* (*small*) also achieves the best results. For PAI-3DMM, we are able to balance the tradeoff between the model’s reconstruction accuracy and model size by adjusting the subspace dimension.

4.3. Ablation test

As mentioned in section 3.1, the initial ordering of node’s neighbors, i.e., $\{x_{i,1}, \dots, x_{i,|\mathcal{N}_i|-1}\}$, is random and without specified. In order to evaluate the robustness and effectiveness of PAI-Conv, we reshuffle the ordering of each node’s neighbors by creating a randomized index list from 0 to $|\mathcal{N}_i| - 1$. As shown in Table 2, in both DFAUST and COMA datasets, the reconstruction errors produced by the model with reshuffling each node’s neighbors are very close to the baseline. Thus, the learnable soft-permutation matrix in our PAI-Conv for each node is robust to the initial neighbor ordering. PAI-Conv is easy to be implemented without involving into any manual design for the local coordinate systems and archives remarkable results on 3D shapes.

Table 2 also shows the impact of initialization methods for the soft-permutation matrices. In baseline and “*Random init of P*”, we initialize the soft-permutation matrices with identity matrix and randomly from uniform distribution, respectively. Random initialization for the soft-permutation matrices degrades the model’s performance. This is because random initialization will neutralize each node’s neighbors at the beginning of training and make each node’s neighbors indistinguishable, resulting in difficulty of extracting local features of 3D shapes.

In our experiments, we set the neighbor size $K = 9$. The effect of the neighbor size on PAI-3DMM is shown in Figure 6. The reconstruction error decreases and model size increases when increasing the neighbor size. Compared to Table 1, when the neighbor size $K = 5$, the reconstruction error (3.869) are still better than PCA (9.977), COMA (5.238), and Spiral (5.258). In practice, we can choose a neighbor size to balance the tradeoff between the reconstruction accuracy and model size.

5. Discussion

In this work, we propose a new convolutional operation for 3D shape representation learning and demonstrate its

Table 2. Ablation tests of PAI-3DMM with the latent size $d = 32$. “*Reshuffle neighbors*” means we reshuffle the ordering of each node’s neighbors randomly. “*Random init of P*” means we initialize the soft-permutation matrices randomly from uniform distribution.

METHOD	DFAUST (MM)	COMA (MM)
Our baseline	3.492	0.117
RESHUFFLE NEIGHBORS	3.527	0.117
RANDOM INIT OF P	4.488	0.137

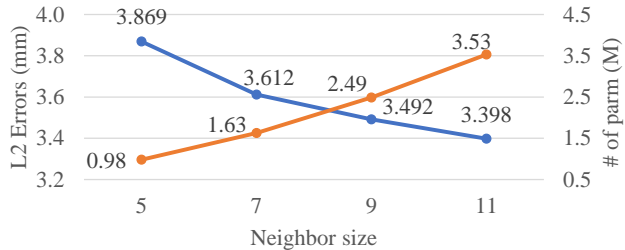


Figure 6. Comparison of different neighbor sizes of our PAI-3DMM on DFAUST dataset when the latent size $d = 32$. The blue line represents the reconstruction error and orange line represents the model’s parameter number.

performance on 3D shape generation tasks. Using the same architecture of convolutional mesh autoencoder, our model achieves significant improvement in 3D shape reconstruction accuracy compared to state-of-the-art methods.

Since 3D graph data are irregular, we use learnable soft-permutation matrices to resample each node’s neighbors and apply shared anisotropic filters across all the nodes. The proposed permutable anisotropic convolution is called PAI-Conv. Compared to previous convolutional operations that either use isotropic filters (e.g., ChebNet and GCN) or use anisotropic filters with predefined local coordinate systems (e.g., Spiral-Conv and MoNet), PAI-Conv is able to extract local features depending on the geometric shape of each node and has much better representation power.

In this paper, we choose the node’s one-ring neighborhood for PAI-Conv operation according to the graph’s edge connections. However, the definition of PAI-Conv does not limit how to select each node’s neighbors. For example, we can use K -nearest neighbors (KNN) as each node’s neighbors, in which way the edge connections are unnecessary so that PAI-Conv can further be extended on point cloud data. Another possible extension of PAI-Conv is instead of learning each node’s soft-permutation matrix directly, we can design a distance metric between the node and its neighbors to determine the soft-permutating matrix. In the future, other than 3D shape data, the effectiveness of PAI-Conv on other graphs, such as social networks, molecules, multi-agent systems, etc., will be explored.

References

- Atwood, J. and Towsley, D. Diffusion-convolutional neural networks. In *Proceedings of the 30th International Conference on Neural Information Processing Systems, NIPS16*, pp. 20012009, Red Hook, NY, USA, 2016. Curran Associates Inc. ISBN 9781510838819.
- Blanz, V. and Vetter, T. A morphable model for the synthesis of 3D faces. In *Proceedings of the 26th Annual Conference on Computer Graphics and Interactive Techniques, SIGGRAPH 99*, pp. 187194, USA, 1999a. ACM Press/Addison-Wesley Publishing Co. ISBN 0201485605. doi: 10.1145/311535.311556.
- Blanz, V. and Vetter, T. A morphable model for the synthesis of 3D faces. In *Proceedings of the 26th Annual Conference on Computer Graphics and Interactive Techniques, SIGGRAPH '99*, pp. 187–194, New York, NY, USA, 1999b. ACM Press/Addison-Wesley Publishing Co. ISBN 0-201-48560-5. doi: 10.1145/311535.311556.
- Bogo, F., Romero, J., Pons-Moll, G., and Black, M. J. Dynamic FAUST: Registering human bodies in motion. In *The IEEE Conference on Computer Vision and Pattern Recognition (CVPR)*, July 2017.
- Boscaini, D., Masci, J., Rodolà, E., and Bronstein, M. Learning shape correspondence with anisotropic convolutional neural networks. In Lee, D. D., Sugiyama, M., Luxburg, U. V., Guyon, I., and Garnett, R. (eds.), *Advances in Neural Information Processing Systems 29*, pp. 3189–3197. Curran Associates, Inc., 2016.
- Bouritsas, G., Bokhnyak, S., Ploumpis, S., Bronstein, M., and Zafeiriou, S. Neural 3D morphable models: Spiral convolutional networks for 3D shape representation learning and generation. In *The IEEE International Conference on Computer Vision (ICCV)*, October 2019.
- Bruna, J., Zaremba, W., Szlam, A., and LeCun, Y. Spectral networks and locally connected networks on graphs. In *2nd International Conference on Learning Representations, ICLR 2014, Banff, AB, Canada, April 14-16, 2014, Conference Track Proceedings*, 2014.
- Cao, C., Hou, Q., and Zhou, K. Displaced dynamic expression regression for real-time facial tracking and animation. *ACM Trans. Graph.*, 33(4):43:1–43:10, July 2014a. ISSN 0730-0301.
- Cao, C., Weng, Y., Zhou, S., Tong, Y., and Zhou, K. Face-warehouse: A 3D facial expression database for visual computing. *IEEE Transactions on Visualization and Computer Graphics*, 20(3):413–425, March 2014b. ISSN 1077-2626. doi: 10.1109/TVCG.2013.249.
- Clevert, D.-A., Unterthiner, T., and Hochreiter, S. Fast and accurate deep network learning by exponential linear units (elus). *arXiv preprint arXiv:1511.07289*, 2015.
- Defferrard, M., Bresson, X., and Vandergheynst, P. Convolutional neural networks on graphs with fast localized spectral filtering. In Lee, D. D., Sugiyama, M., Luxburg, U. V., Guyon, I., and Garnett, R. (eds.), *Advances in Neural Information Processing Systems 29*, pp. 3844–3852. Curran Associates, Inc., 2016.
- Genova, K., Cole, F., Maschinot, A., Sarna, A., Vlastic, D., and Freeman, W. T. Unsupervised training for 3D morphable model regression. In *The IEEE Conference on Computer Vision and Pattern Recognition (CVPR)*, June 2018.
- Hamilton, W., Ying, Z., and Leskovec, J. Inductive representation learning on large graphs. In Guyon, I., Luxburg, U. V., Bengio, S., Wallach, H., Fergus, R., Vishwanathan, S., and Garnett, R. (eds.), *Advances in Neural Information Processing Systems 30*, pp. 1024–1034. Curran Associates, Inc., 2017.
- Kalogerakis, E., Hertzmann, A., and Singh, K. Learning 3D mesh segmentation and labeling. New York, NY, USA, 2010. Association for Computing Machinery. ISBN 9781450302104.
- Kingma, D. P. and Ba, J. Adam: A method for stochastic optimization. *arXiv preprint arXiv:1412.6980*, 2014.
- Kipf, T. N. and Welling, M. Semi-supervised classification with graph convolutional networks. In *International Conference on Learning Representations (ICLR)*, 2017.
- Li, R., Wang, S., Zhu, F., and Huang, J. Adaptive graph convolutional neural networks. In *Thirty-Second AAAI Conference on Artificial Intelligence*, 2018.
- Lim, I., Dielen, A., Campen, M., and Kobbelt, L. A simple approach to intrinsic correspondence learning on unstructured 3D meshes. In *The European Conference on Computer Vision (ECCV) Workshops*, September 2018.
- Loper, M., Mahmood, N., Romero, J., Pons-Moll, G., and Black, M. J. SMPL: A skinned multi-person linear model. *ACM Trans. Graphics (Proc. SIGGRAPH Asia)*, 34(6):248:1–248:16, October 2015.
- Masci, J., Boscaini, D., Bronstein, M. M., and Vandergheynst, P. Geodesic convolutional neural networks on riemannian manifolds. In *The IEEE International Conference on Computer Vision (ICCV) Workshops*, December 2015.
- Monti, F., Boscaini, D., Masci, J., Rodola, E., Svoboda, J., and Bronstein, M. M. Geometric deep learning on graphs

and manifolds using mixture model CNNs. In *The IEEE Conference on Computer Vision and Pattern Recognition (CVPR)*, July 2017.

Paysan, P., Knothe, R., Amberg, B., Romdhani, S., and Vetter, T. A 3D face model for pose and illumination invariant face recognition. In *2009 Sixth IEEE International Conference on Advanced Video and Signal Based Surveillance*, pp. 296–301, Sep. 2009. doi: 10.1109/AVSS.2009.58.

Qi, C. R., Su, H., Mo, K., and Guibas, L. J. PointNet: Deep learning on point sets for 3D classification and segmentation. In *The IEEE Conference on Computer Vision and Pattern Recognition (CVPR)*, July 2017.

Ranjan, A., Bolkart, T., Sanyal, S., and Black, M. J. Generating 3D faces using convolutional mesh autoencoders. In *The European Conference on Computer Vision (ECCV)*, September 2018.

Romero, J., Tzionas, D., and Black, M. J. Embodied hands: Modeling and capturing hands and bodies together. *ACM Transactions on Graphics, (Proc. SIGGRAPH Asia)*, 36 (6), November 2017.

Tran, L. and Liu, X. Nonlinear 3D face morphable model. In *The IEEE Conference on Computer Vision and Pattern Recognition (CVPR)*, June 2018.

Veličković, P., Cucurull, G., Casanova, A., Romero, A., Liò, P., and Bengio, Y. Graph Attention Networks. *International Conference on Learning Representations*, 2018. accepted as poster.

Xie, J., Zheng, Z., Gao, R., Wang, W., Zhu, S.-C., and Nian Wu, Y. Learning descriptor networks for 3D shape synthesis and analysis. In *The IEEE Conference on Computer Vision and Pattern Recognition (CVPR)*, June 2018.

Zhu, X., Lei, Z., Yan, J., Yi, D., and Li, S. Z. High-fidelity pose and expression normalization for face recognition in the wild. In *2015 IEEE Conference on Computer Vision and Pattern Recognition (CVPR)*, pp. 787–796, June 2015. doi: 10.1109/CVPR.2015.7298679.

Zhuang, C. and Ma, Q. Dual graph convolutional networks for graph-based semi-supervised classification. In *Proceedings of the 2018 World Wide Web Conference, WWW 18*, pp. 499508, Republic and Canton of Geneva, CHE, 2018. International World Wide Web Conferences Steering Committee. ISBN 9781450356398. doi: 10.1145/3178876.3186116.